Proceedings of COBEM 2009
20th International Congress of Mechanical Engineering
November 15-20, 2009, Gramado, RS, Brazil

Recent Developments in Multi-Hole Probe (MHP) Technology

Demetri Telionis, telionis@vt.edu

Yihong Yang, yhyang@vt.edu

Virginia Polytechnic Institute and State University Blacksburg, VA, 24060 USA

Othon Rediniotis, rediniotis@tamu.edu

Texas A&M University, College Station, Texas, 77843 USA

Abstract. *Multi-hole probes are fluid flow instruments that measure pressure along pressure ports arranged on their tips. With proper calibration, this information can then return three components of the fluid velocity as well as static and dynamic pressure. With the development of modern methods like laser-Doppler velocimetry, particle-image velocimetry and others, the use of these probes has declined. But the emergence of miniature pressure sensors and modern electronics new multi-hole probes were designed and tested to match some of the features of other methods. Moreover, multi-hole probes are robust, and can sustain harsh environments, like very high temperatures, opaque fluids, flows carrying particulates and others. Moreover, they are easier to use and less expensive. In the present paper we review recent developments in multi-hole probe technology, namely, instrumentation and calibration methods that increase the probe's frequency response, allow them to take data in wide ranges of the Mach number, and correct for inertial effects. We also present examples of using these probes in many industrial settings.*

Keywords: *Multi-hole probe, turbulence measurements, pressure measurements, wind-speed measurements, subsonic/supersonic measurements*

1. INTRODUCTION

In the first few decades of aerodynamics research, the classical Pitot-static tube was extensively used to measure the velocity in a stream. And for decades again, pressure manometers have been employed to measure the difference between stagnation and static pressure, and thus allow the calculation of the velocity, if the density of the fluid was known. A Pitot-static tube can generate accurate measurements if the flow is uniform and if the probe is nearly aligned with the direction of the flow velocity. Both requirements represent significant limitations for the measurement of the velocity at a point within a flow field. But Pitot-static probes are still extensively used in situations where the direction is known a priori, or if the direction of the flow does not change significantly locally. These limitations will be discussed in some detail later in this paper. The design of modern Multi-Hole Probes (MHP) for the measurement of flow velocity is based on the principle of operation of a Pitot-static tube.

The multi-hole pressure probe is a proven and mature measurement technology to resolve the 3-dimensional velocity vectors in steady flow fields (Bryer and Pankhurst 1971, Everett and Gerner 1983, Rediniotis et al. 1993, Zilliac 1989). What could not be measured until very recently is the pressure in midfield. But today, many years after the development of sophisticated methods of measurement like Hot-Wire Anemometry (HWA), Laser-Doppler Velocimetry (LDV) and Particle-Image Velocimetry (PIV), we turned again to the principles of a Pitot-static tube to

return the in-field static pressure. This can now be achieved with multi-hole probes properly calibrated. In fact MHP are the only probes that can provide the local value of all three components of the velocity, both static and dynamic pressure and with the appropriate modifications the total and static temperature and the local composition of the fluid. The present article is devoted to recent developments in multi-hole probe technology.

Multi-hole probes are based on the fact that the static pressure varies over a solid surface immersed in the flow, from the maximum value, which is equal to the stagnation pressure to low values the order of the base pressure in the wake of the body. Measuring the pressure at distinct points over the body of a probe can provide all the necessary information on velocity components and in-field pressures. This requires careful calibration. Many different shapes have been employed for the tip of a MHP as for example cones, spherical or cylindrical surfaces or faceted surfaces. These probes must be inserted in the flow at the point where a measurement is required. They therefore provide point measurements. And they interfere with the flow. Probe interference is in principle calibrated out, but as discussed later, there are limitations that depend on the dimensions of the tip and the local spatial variations of the flow. These topics will be discussed in some detail in the present article.

Hot-Wire Anemometry (HWA), Laser-Doppler Velocimetry (LDV) and Particle-Image Velocimetry (PIV) are tools described in great detail in literature. HWA and LDV are also point instruments, whereas PIV can generate information along a plane cutting across the velocity field of consideration. Point instruments require traversing along the domain of interest to map out a velocity field. Of all these methods, the hot wire anemometer is the most vulnerable to particulates in the flow and can easily be damaged if not handled properly. It is therefore not appropriate for industrial applications. LDV and PIV require optical access to the point of measurement, which is a limitation to the experimental rig, as well as the range of working media. MHP are robust and reliable tools most appropriate for many industrial applications, that can be operated in opaque fluids that could carry some particulates, and do not need optical access to the point of measurement. But in some cases they may introduce some local or even global interference to the flow.

Here we first discuss the principles and the geometrical configurations of different MHP designs. Calibration is a significant element of MHP and the difficulties associated with it are discussed next. But it is important to mention here that MHP calibrations do not have to be repeated, unless the probe tip is damaged. We then present discussions of probe interference with the flow, with surface walls and with multiple probes. Finally turbulence measurements and examples of applications are presented.

2. THE MULTI-HOLE PROBE (MHP) – PRINCIPLE OF OPERATION AND DESIGNS

2.1. The MHP Principle of Operation

When a body is inserted in the flow of any fluid, the pressure distribution over its surface varies from a maximum at the stagnation point to some low values that are often lower than the static pressure far upstream. For bluff bodies, the maximum pressure is equal to the total pressure, p_o which is the sum of the static pressure, p_∞ and the dynamic pressure far from the body.

$$p_o = p_\infty + \rho V_\infty^2/2 \qquad (2.1)$$

The lowest pressures are found near the regions where the inclination of the surface of the body is nearly parallel to the free stream. This of course is not always true. The flow over bluff bodies often separates. Flow separation alters the local pressure distribution and introduces adverse pressure gradients in regions where the slope of the surface of the body is decreasing but not yet zero. As a result for example, for laminar flow over a circular cylinder, separation occurs at about 80^o from the point of stagnation, rather than at 90^o where the tangent to the surface is parallel to the free-stream velocity.

The principle of multi-hole probe measurements is based on the fact that if a bluff body is immersed in a stream, the pressure at specific points on its surface is related to the direction and magnitude of the stream velocity. This relationship can be developed analytically, but in practice probes are calibrated experimentally.

In this article "far upstream", "free stream", and "conditions at infinity", denoted by the subscript ∞ imply a position upstream of the probe tip, where we assume that the flow is uniform and unaffected by the presence of the probe. These assumptions will need qualification. But in practice, this distance is the order of the probe tip diameter. We assume that the local flow nonuniformities, like sharp curvature of streamlines or large velocity gradients are small compared to the disturbances generated by the probe. This hypothesis allows us to use MHP to measure the velocity and pressure at a point in a flow field that develops in space.

To demonstrate the principle, consider a pitch probe consisting of a circular cylinder with pressure taps 1,2 and 3 along the meridional angles at θ=0, 45^o and -45^o as shown in Fig. 1. If the free stream is approaching in the horizontal direction assumed to be normal to the axis of the cylinder, the pressure reading at θ=0 will be the stagnation pressure and the readings along the other two pressure taps will be equal to each other. If this probe is inserted in a two-dimensional field inclined with respect to the probe's axis by an angle α, which in this article will be referred to as the incidence angle, then pressure measurements at points θ=0, 45^o and -45^o can return the free-stream velocity magnitude V_∞, the incidence angle, as well as the static and dynamic pressure. This can be demonstrated analytically.

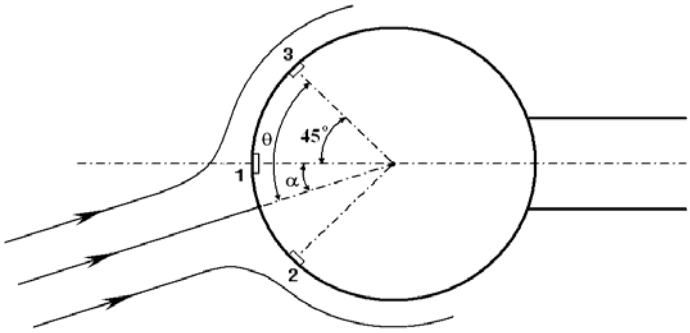

Figure 1. A very simple pitch/magnitude three-hole probe

For incompressible flow, the pressure and velocity at a point on the body, p, V are related to the pressure and velocity far from the body, p_∞, V_∞ by

$$p_\infty + \frac{\rho}{2} V_\infty^2 = p + \frac{\rho}{2} V^2 \tag{2.2}$$

For a circular cylinder, the potential flow solution gives the velocity on the cylinder as

$$V(\theta) = 2V \sin\theta \tag{2.3}$$

where θ is the angular distance from the point of stagnation to the point of interest.

We can then employ Eqs. (2.2) and (2.3) for the pressure at the three pressure taps as follows:

$$P_\infty + \frac{\rho}{2} V_\infty^2 = P(45^\circ - \alpha) + 2\rho V_\infty^2 \sin^2(45^\circ - \alpha) \tag{2.4}$$

$$P_\infty + \frac{\rho}{2} V_\infty^2 = P(\alpha) + 2\rho V_\infty^2 \sin^2 \alpha \tag{2.5}$$

$$P_\infty + \frac{\rho}{2} V_\infty^2 = P(45^\circ + \alpha) + 2\rho V_\infty^2 \sin^2(45^\circ + \alpha) \tag{2.6}$$

If the pressure at ports 1, 2 and 3 are measured, then the system of Eq. (2.4) to Eq. (2.6) can be solved for the unknowns p_∞, V_∞ and α, which are the local value of the static pressure, the local magnitude of the velocity and the slope of this velocity vector.

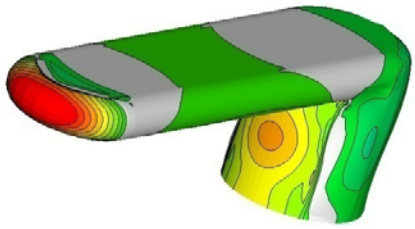

Figure 2. Pressure distribution over probe with race-track cross section. Largest values correspond to deep red, and the lowest to green

The basic idea is now to design a probe with a tip shape that will involve measurable variations of the pressure that can be associated with the direction and magnitude of the local velocity vector. Pressure taps are placed along the tip of the probe at locations that will involve measureable variations of the local pressure, associated with the magnitude and direction of the flow. In Fig. 2 we present numerical results of the pressure distribution over a probe with a race-track cross section, which is recommended to detect the incidence angle in a plane normal to the stem axis. These results were obtained for zero incidence. The highest pressure is indicated by the deepest red. With three pressure taps (not shown in this figure), one along the center of the tip and two on each side, this probe can be used to detect the incidence angle.

Analytical or numerical relations similar to those represented by Eq. (2.4) to Eq. (2.6) connecting pressure values on the probe tip to the local velocity, static and dynamic pressure can be derived for any probe tip shape. But minute errors in the machining of the probe tip and the location of the pressure taps introduce measurement errors that can only be eliminated by calibration. Probe calibration requires inserting the probe in a known uniform flow field, traversing it along pitch and yaw angles and measuring the corresponding pressures. Calibration processes are discussed later in this paper.

2.2. One-, Three-, Five-, Seven-, Twelve-, and Eighteen-Hole Probes

The number of holes at the tip of the probe, or further back enables a probe to return the incidence angles with the desired accuracy. The larger the number of holes, the better the accuracy of a probe to detect the direction of the flow at larger angles of incidence. Roughly Pitot-static probes are limited to incidence angles less than 10 degrees, five-hole probes are limited to 55 degrees and seven-hole probes to 75 degrees. For incidence angles larger than 75 degrees, one needs a twelve- or an eighteen-hole probe.

The number of holes is not directly associated with the number of necessary sensors. As described later, the classical Pitot-Static is equipped with seven holes, but six of them open to a chamber where the pressure settles to the average of the ambient static pressure. One then needs just two sensors to measure the total and static pressure, or just one differential pressure sensor.

The standard Pitot-static probe can be classified as a MHP. This probe is a tube with a single hole along the tip, and six or eight holes along a ring, known as the static ring, six to ten diameters from the tip. In most structural designs, the probe consists of a metal tube, with one small pipette connected to the port on the tip of the probe. The static ring holes lead to the interior of the probe body. If the probe is aligned with the stream, then the disturbance induced to the flow by the probe is negligible along the static ring, and both the pressure and velocity there return to their upstream value. The static pressure inside the probe chamber is equal to the static pressure, p_∞. It has been shown that for small inclinations of the probe axis, the order of 5 degrees with respect to the free stream, the pressure tap on its tip still records the total pressure of the stream with an error of less than 1%. The pressure along the pressure ring varies, with the highest pressure along the windward side, with respect to the velocity cross flow and the lowest along the lee side. As it turns out, the average of the pressures recorded by the pressure taps along the static ring is very close to the static pressure far from the probe. This averaging process is carried out quite well, by allowing all static ring pressure taps to communicate with the interior chamber. A Pitot-static probe is therefore forgiving, and could provide a good measurement of the magnitude of the velocity even if the probe is not perfectly aligned with the stream.

If three holes are arranged on the same plane as shown, then the probe can detect the angle that the axis of the probe makes with the projection of the flow velocity on the probe plane. In cases that the flow velocity component normal to this plane is very small, this probe becomes a yaw probe. A static ring allows this instrument to be a stand-alone probe to detect the magnitude and direction of the oncoming stream over a vehicle that is moving on a flat ground. In the laboratory, such probes are useful in situations where the flow is nominally two-dimensional. This is the case when the flow is constrained by two walls, but then a static ring may not measure accurately the static pressure.

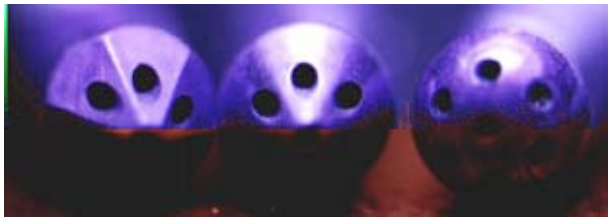

Figure 3. Faceted, conical and hemispherical seven-hole tips

The most common multi-hole probes are the five-hole and the seven-hole probes. Holes are arranged along the tip of the probe as shown in Fig. 3. Many tip shapes have been used, the most common of which are faceted, conical or hemispherical,. The principle described in Section 2.1 can easily be extended to three-dimensional flow. It all depends on the fact that the highest pressure occurs at the point of stagnation and the pressure on the surface of the probe tip decreases with distance from this point. For a sphere, one can derive unique mathematical relations that connect the pressure at the pressure taps with the direction and the magnitude of the velocity as functions of the location of the pressure taps. This is essentially a generalization of Eqs. (2.4-2.6).

For a hemispherical probe, one may assume that the pressure on the front of the probe is essentially the same with the pressure over a sphere. The potential flow solution is then a very good approximation for this flow, and the pressure depends only on the angular distance, θ from the stagnation point. The pressure coefficient becomes. If a probe with a spherical tip is immersed in the flow, the pressure at a point on its surface depends only on the cone angle, θ between the probe axis and the point of interest

$$C_p = \left(\frac{9}{4}cos^2(\theta) - \frac{5}{4}\right) \tag{2.7}$$

Let the cone angle between the center of the probe, C and the point of interest P be θ_{CP}, as shown in Fig. 2.6. This angle defines the probe geometry and is usually the same for all pressure ports. If the probe is now given a pitch angle denoted in Fig. 2.6 by θ_{CX} and a roll angle, φ, then the cone angle between the point of stagnation X and the point of the pressure tap, θ_{CP} is the angle that if substituted in Eq. (2.7) will return the pressure at this point. There is an analytical solution for θ_{CP} in terms of all the other angles, given by the following equation

$$\theta_{XP} = 2sin^{-1}\left[\left(sin(\frac{\theta_{CP}}{2})^2 + sin(\frac{\theta_{CX}}{2})^2 - 2sin\,(\frac{\theta_{CP}}{2})sin\,(\frac{\theta_{CX}}{2})cos\,(\emptyset_{XP})\right)^{-1/2}\right] \tag{2.8}$$

Given the pressures along points on the sphere, these two equations can be solved to determine pitch and roll of the probe.

In practice, there are no analytical solutions for tip geometries other than the sphere, and therefore these relationships should be determined only by calibration. But as explained earlier, the main reason that dictates

calibration of every single probe is the fact that minute imperfections in the machining of the probe tip result in significant differences of the calibration surfaces. Extended calibrations of conical five-hole probes and seven-hole probes indicate that they can provide good accuracy for incidence angles up to 55 degrees and 75 degrees respectively.

Probes that can sense and measure direction and magnitude of the flow approaching with incidence angles as large as 150 degrees have been designed. These are essentially spheres with 12 or 18 holes attached to a cylindrical stem. It is the presence of the stem that is now limiting the incidence angle.

2.3. Tip/Stem Shapes and Pressure Measurements

Theoretically, any tip shape would work for a multi-hole probe. The principle criterion to determine the proper shape for a specific application is that the pressure recorded by a pressure tap should vary smoothly with the incidence angle. This is because sharp changes on the calibration curve, $\Delta p/\Delta\alpha$ or any of the other angles, could introduce inaccuracies in the angles that the probe reads.

A large number of tip shapes have been employed with acceptable results. Most common among them are the cone and the hemisphere. But faceted, i.e. tips with flat surfaces also indicate quite good performance. The difference in the performance of smooth versus faceted tips is due to the flow separation characteristics. Separation over smooth surfaces is gradual, and displaces smoothly over the surface, which is an attractive feature for a MHP. However, the calibration curves may display some abrupt changes as the free-stream velocity increases, because the Reynolds number also increases, and induces transition to turbulent separation, which moves the point of separation further downstream. The sharp corners of a faceted tip force separation alone the corner, and therefore the calibration curves are not as sensitive to changes of the Reynolds number. However the flow over faceted shapes is almost always separated, and therefore more sensitive to unsteady stall effects as described later, which introduce errors in detecting dynamic phenomena. Typical work were done by Heneka (1983) and Gossweiler (1993) respectively.

The pressure taps arranged at the tip of a probe must communicate with pressure sensors. Small metal tubes attached to each pressure tap lead to the sensitive element of pressure sensors. The metal tubes are often stepped into plastic tubes (Tygon tubing). The length of these tubes can vary and can be as long as several meters. But the damping of pressure fluctuations increases with the length of these tubes and limits the measurements to mean values. For short tubes, acoustic calibrations discussed earlier provide correction factors that would allow multi-hole probes to resolve signals with frequency responses as high as a few hundred of Hertz. But to increase the frequency response to levels comparable to LDV and PIV, the sensors must be places as close as possible to the pressure taps. This means that the pressure sensors must be imbedded in the body of the probe, or placed flush on the surface of the tip of the probe.

2.4. Acoustic Properties of Tubing and Experimental Correction

Instrumenting a model as discussed in Section 2.1 can provide the average pressure over a model. If the pressure over the model is fluctuating in time, these arrangements can not be used to provide the instantaneous pressures over

the model. The pressure signals can be amplified or attenuated through the flexible hoses, and require special attention to return the true pressure fluctuation on the surface of the model. Connections between the tip of a multi-hole probe and the measuring sensors require similar attention.

Figure 4. shows a schematic of a basic system consisting of a pressure measuring transducer connected to a tubing system of length L and diameter 2r. The true pressure at the measurement point is indicated by $p_s(t)$ while the pressure measured by the transducer is denoted by $p_r(t)$. The pressure at the transducer will be distorted in amplitude and phase, due to the compressibility of the medium and thus the presence of viscous flow inside the tubing. This distortion depends on several factors, the most important of which are: inner tubing diameter, tubing length, volume V in front of the pressure sensor and medium properties such as viscosity and density.

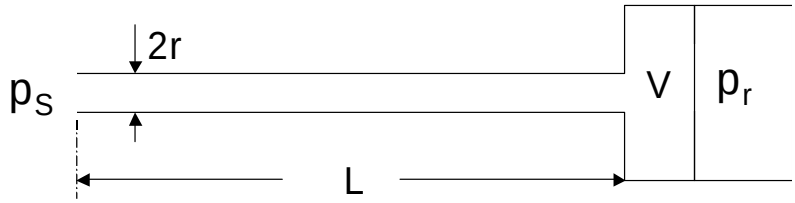

Figure 4. Schematic of a basic multi-hole probe tubing system, with inlet pressure $p_s(t)$, tube, transducer volume (V) and pressure transducer with measurement $p_r(t)$

For example, for a tubing system consisting of a 53 mm long, 0.25 mm ID steel tube, and an Endevco transducer, we show in Figure 5. the signal amplitude distortion as a function of frequency. At high frequencies massive attenuation is observed.

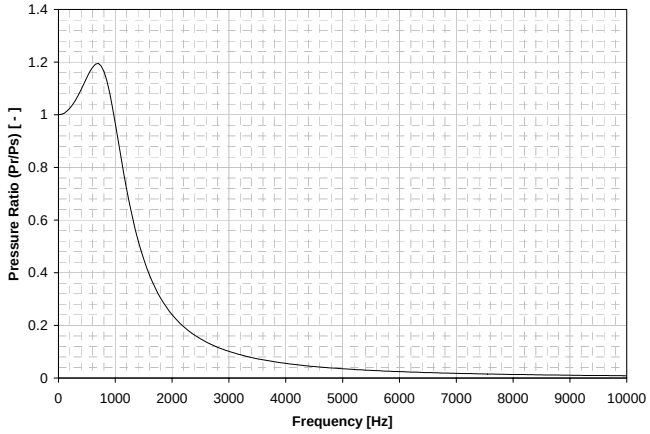

Figure 5. Amplitude ratio for a 53 mm long, 0.25 mm ID steel tube in air at standard conditions

Based on the large uncertainty and tolerances in small diameter tubing systems, an accurate theoretical model of the transfer function is nearly impossible to attain. Therefore, an experimental calibration system is needed. Rediniotis and Pathak (1999) develop a simple system for such calibrations shown in Fig. 6. This system generates a

repeatable fluctuating pressure at the inlet of the tubing system, while continuously monitoring the inlet pressure (p_s) and the pressure at the receiving end of tubing system (p_r). A loudspeaker was chosen as the driver for the system, and was mounted with its membrane facing a plate, forming a closed cavity. Two holes in the plate equidistant from the center of the loudspeaker and 25.4 mm apart are used to mount the reference transducer (p_s) and the tubing system.

The loudspeaker was used to generate a sinusoidal pressure signal in the cavity with accurately set frequency and amplitude. Determination of the transfer function of the tubing system necessitates that the frequency is scanned through a range of values. At each separate frequency, the ratio p_r/p_s was calculated as well as the phase angle between the two signals. A PID loop continuously monitored the reference pressure p_s and adjusted the voltage supplied to the loudspeaker to maintain constant RMS pressure amplitude in the cavity. The pressure level produced by the loudspeaker at low frequencies (<500 Hz) was in the range of 800 Pa RMS. However, at higher frequencies (>2 kHz), the maximum was approximately 30 Pa RMS.

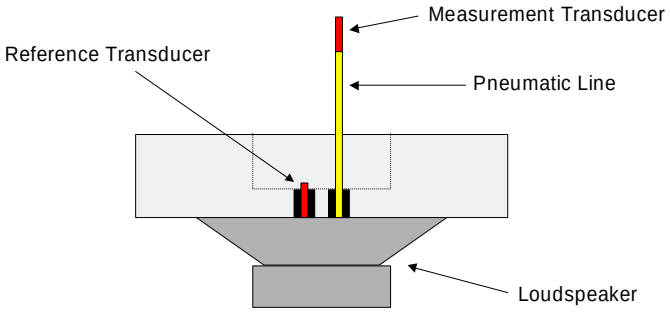

Figure 6. Calibration facility to determine the transfer function for tubing systems

The purpose of such a procedure is to accurately reconstruct the instantaneous pressure at the inlet of the tubing system. Pressure tubing systems that incorporate long tubes, such as those encountered in aircraft instrumentation, and multi-hole probes with external pressure transducers, are generally over-damped. In a pressure reconstruction procedure for such systems, the attenuation and time lag can be theoretically predicted by simple equations. A post-processing pressure reconstruction procedure can readily be formulated. A similar method outlined in Paniagua and Denos (2000) promises to reconstruct the pressure signal with high accuracy. This method, or the simpler model outlined by Rediniotis and Pathak (1999), is conveniently used for over-damped systems. It should be noted that these equations assume over-damped systems, and will not predict the overshoot or resonance that can occur in under-damped systems.

However, for a general system (under-damped or over-damped) a general pressure reconstruction procedure is needed, like the one illustrated in Fig. 7, which includes a windowing function and a frequency smoothing function. The smoothing function was based on a two-pass recursive routine to eliminate frequency-shift distortions. FFT transforms assume that the signal is periodic within the sample set. The purpose of a windowing function is to reduce leakage for signals that are not perfectly periodic within the sample. The windowing function will force the beginning and the end of a sample set to zero, imposing quasi-periodicity to the data. There are a number of standard

windowing functions, some have better characteristics than others when it comes to maintaining magnitude accuracy (e.g. flattop) and phase accuracy (e.g. Hanning). Some tests might be self-windowing, meaning that the value is zero at both ends of the sample set. Periodic signals can, with careful timing, be recorded such that the first point in the sample set is equal to the N+1 point, and no windowing function would be necessary.

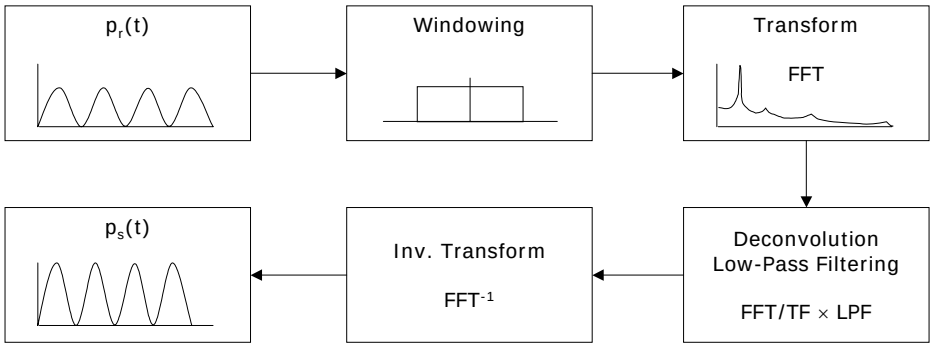

Figure 7. Pressure reconstruction routine

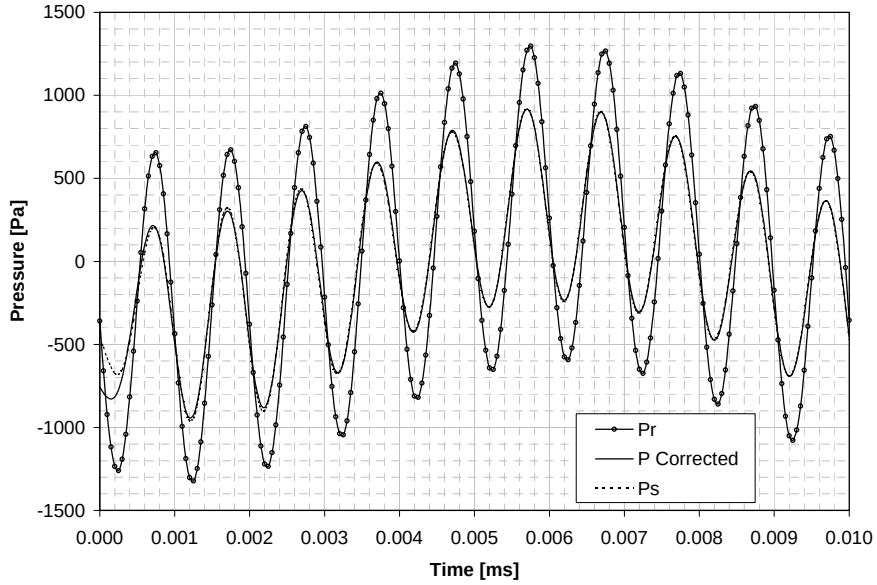

Figure 8. Measured (Pr), true (Ps), and corrected (Pcorr) pressure signals for 100 Hz + 1000 Hz test case

Rediniotis and Pathak (1999) used a uniform window and found that no smoothing function was required to correct for frequency distortions. The deconvolution procedure was performed by dividing the FFT spectrum by the transfer function of the tubing system. The corrected spectrum was further multiplied with a low-pass filter, forcing all spectrum values above the cut-off frequency to zero. The spectral reconstruction routine was tested on data

generated by the loudspeaker facility. This facility can be used to generate continuous pressure signals with various waveforms. For these signals, both the reference pressure (p_s) and the measured pressure at the end of the tubing system (p_r) were recorded. The pressure reconstruction routine was then used to correct the measured pressure (p_r) and compared it to the reference pressure (p_s).

An example of pressure reconstruction is presented below. The tested tube was 38 mm long with an inner diameter of 0.5 mm. A test case based on a 100 Hz and a 1000 Hz sine wave was corrected using the described procedure. Figure 8 shows the measured and reference pressures. Large amplification in the pressure and a small shift in the phase angle are observed. The reconstructed pressure is seen to follow the reference pressure accurately.

3. CALIBRATION PROCEDURES

As with any instrument, calibration of MHP requires that the probe is exposed to a series of combinations of parameter values it will be required to read, the data are stored, and the mathematical operation is prepared for the use of the instrument as a measuring device. The physical quantities that the user expects to obtain are the magnitude and the direction of the flow, the static and the dynamic pressure at the point of measurement. All these quantities are functions of the pressures measured by the pressure taps arranged on the tip of the probe. A typical numbering of the tip pressure taps for a five-hole probe is shown in Fig. 9.

The orientation of a probe with respect to the oncoming free stream is defined in terms of two angles. These could be cone and roll, θ and φ, or pitch and yaw, α β, as defined in Fig. 10. The systems *(θ,φ)* and *(α,β)* are completely interchangeable, and the conversion between them is given by the following geometrical relations:

$$\alpha = tan^{-1}(tan\theta sin\emptyset), \quad \beta = sin^{-1}(sin\theta cos\emptyset) \tag{3.1}$$

The calibration data are actually discrete data. When the instrument is used as a measurement tool, the measured quantities fall between the discrete calibration data. Special software is needed for the efficient interpolation that can return measurements in terms of the calibration files.

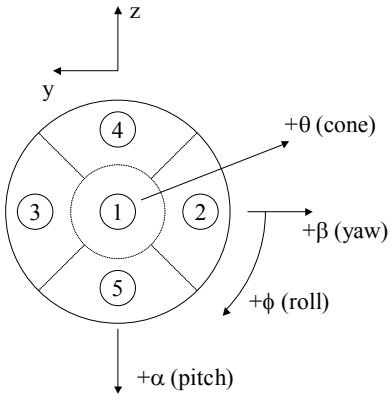

Figure 9. Typical numbering of tip pressure tap for five-hole probe

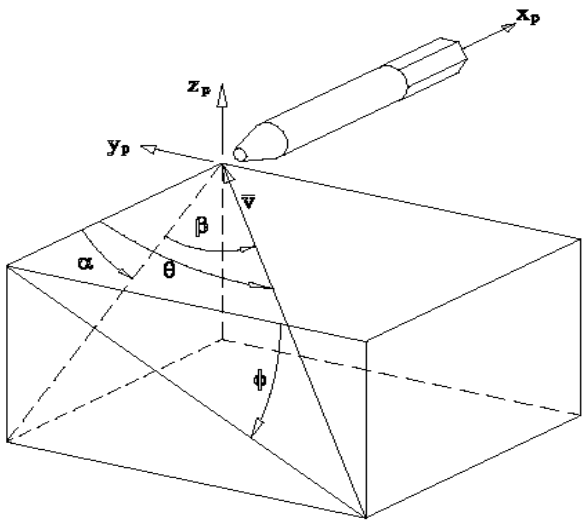

Figure 10. Angles defining the orientation of a probe with respect to the free stream V. Here θ and φ are the cone and roll angles, and α and β are the pitch and yaw angles.

As explained in the following sections, the basic calibration parameters are the angles that define the orientation of the probe, the Reynolds number and the Mach number. The dependence of the quantities to be measured on the calibration parameters is described in terms of calibration surfaces. These surfaces are unique to each instrument. Even if two probes are machined on computer-controlled equipment with identical specifications and drawings, their calibration surfaces deviate from each other. In other words, no two probes are identical to each other. This is because the slightest mechanical discrepancies on the surface of the probe tips can induce non-negligible differences in the calibration surfaces. This is why each probe must be calibrated through the entire domain of the parameter values that it is expected to encounter.

3.1. Calibration Mechanisms

A calibration machine should be able to generate independently the discrete values of two spatial attitude angles, the Reynolds number, Re and the Mach number, M:

$$Re=\rho V_\infty L/\mu \qquad M= V_\infty/a \tag{3.2}$$

This means that the total temperature and total pressure of the free stream must be known. Such machines must generate free streams with the lowest levels of turbulence possible, and mechanisms that can position the probe at different spatial orientations.

Free streams with varying Reynolds and Mach numbers can be generated by closed-circuit wind tunnels or blow-down wind tunnels. In most facilities, it is not possible to control independently the Mach number and the Reynolds number. This is because if the density and temperature cannot be controlled independently, then increasing

the speed of the tunnel results in increases of both the Reynolds number and the Mach number. To control these parameters independently requires a facility that can be operated at controlled pressures and/or temperatures. Such facilities are too expensive to construct and to operate. For most practical applications, the dependence of the calibration surfaces on the Reynolds number is rather weak. It is therefore adequate to calibrate for different values of the Mach number, and in practice, this is achieved by increasing the speed of the tunnel.

A probe must be placed in the tunnel with its tip as close as possible to the middle of the test section and be given angular displacements such that its tip is not linearly displaced. In other words, the probe tip must remain at the same point in space while its axis is given the required inclinations. This is necessary because even in the most carefully designed tunnels there is some variation of the local velocity vector across the test section.

The most common calibration mechanism that allows adjusting inclination angles keeping the probe tip fixed in space is a U-shaped bracket that can rotate about an axis that passes through its two tips as shown in Fig. 11. One of the U bracket legs is mounted on a stepper motor that controls the cone angle. The other leg is essentially the probe itself, or an extension of it, and this could be mounted at its base on a stepper motor that controls its roll. The base includes a stepper motor to control rolling, indicated by the curly arrow B. The disk G is mounted flash with the wall of the test section, or is placed far from the calibration jet. The roll stepper motor E is placed far from the roll axis, and rolling is achieved by a belt drive.

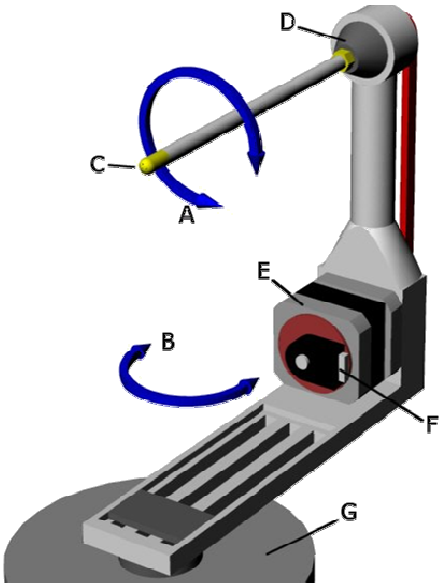

Figure 11. A calibration mechanism with stepper motors to control cone and roll.

3.2. Calibration Mathematical Relations and the Measurement Process

The formulas and the discussion in this article are presented for five-hole probes. But extensions to any number of holes is straightforward and can be found in the literature (Rediniotis et al. 1993, 1999, Johansen et al. 2001). The basic procedure is the following. Measure the five pressures recorded at each of the five holes for a large number of

calibration angles, record the calibration facility static and dynamic pressure and the plenum temperature. Store this information that after calibration should accompany the calibrated probe. Then prepare the software that when the probe is inserted in an unknown flow field, the measured five pressures would return the local value of the total and static pressure and the magnitude and direction of the velocity. The local velocity vector at any measurement location can be fully characterized by four variables. The two angles, pitch α and yaw β, or cone θ and roll ϕ, total pressure coefficient A_t and static pressure coefficient A_s. These quantities are determined as functions of two non-dimensional pressure-coefficients formed from the measured pressures: b_α, b_β or b_θ, b_ϕ .

Consider the numbering of the holes as shown in Fig. 9, which is the front view of the tip of a five-hole probe. Following Johansen (2001) we can then define coefficients in terms of the pressures recorded along the five pressure taps. We start with the definition of a coefficient that will be called the pseudo-dynamic pressure:

$$q = p_1 - \frac{p_2+p_3+p_4+p_5}{4} \tag{3.3a}$$

There is no physical significance of this coefficient, but as will be shown later it will allow us to relate the measured pressures to the quantities we intend to measure. We then define the pitch and yaw coefficients, b_α and b_b and the total and static pressure coefficients, A_t and A_s as follows:

$$b_\alpha = \frac{p_2+p_4-p_5-p_3}{2q} \tag{3.3b}$$

$$b_\alpha = \frac{p_2+p_5-p_3-p_4}{2q} \tag{3.3c}$$

$$A_t = \frac{p_1-p_t}{q} \tag{3.3d}$$

$$A_s = \frac{q}{p_t-p_s} \tag{3.3e}$$

The pitch and yaw coefficients vary with the pitch and yaw angles. But the precise relationships are coupled and can be determined only by the calibration process. As described earlier, the calibration mechanism brings the probe at a sequence of pitch and roll pairs, α and β. The free-stream total and static pressure and the total temperature are recorded, and for each pair, the five pressures p_1 through p_5 are measured. The coefficients b_α, b_β, A_t and A_s are then calculated. In this preprocessing scheme, the probe calibration files are used to create a calibration database that contains for all velocity inclinations all of the dependent and independent non-dimensional coefficients. These data are stored to be used later to measure the velocity vector, the static and the dynamic pressure. These could be thought of as look-up tables where in terms of the values of b_α and b_β , we can find the angles α and β and the values of the coefficients A_t and A_s. One can visualize these functions in terms of surfaces like the one plotted in Fig. 12.

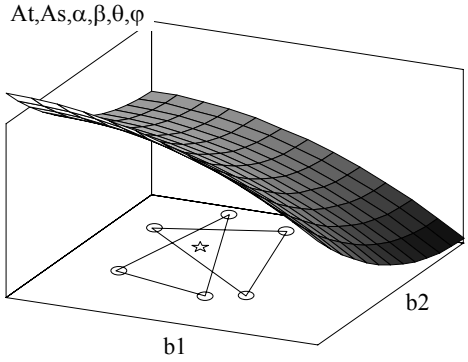

Figure 12. Visualization of calibration coefficients

3.3. Data Reduction Procedure

Once a probe is calibrated, it is ready to be used to determine the flow conditions in an unknown flow field. When the probe is inserted into an unknown flow field the port pressures are recorded and the independent non-dimensional coefficients b_α and b_β are calculated. The second step is to find the closest values of the independent coefficients in the calibration file compared to the test values. In a method proposed by Johansen et al. (2001), calibration points far from the tested point in the b_α and b_β are assumed to have little or no influence on the calculation. Therefore, a local interpolation scheme was used and only calibration points close to the test point were used in the evaluation. A least-squares surface fit technique was employed to calculate the two flow angles and the two pressure coefficients as functions of the independent input variables. The procedure was repeated for A_t and A_s. The selected closest and triangulation-checked calibration points (minimum number determined by the order of the polynomial surface) were used to calculate four separate interpolation surfaces. Each surface was calculated using a polynomial with coefficients calculated by a least-squares approximation method. For a first order surface the following polynomial is used:

$$f(b_\alpha, b_\beta) = a_0 + a_1 b_\alpha + a_2 b_\beta \tag{3.4}$$

Where f can be any of the dependent variables α, β, θ, ϕ, A_t, A_s and a_0, a_1, a_2 are the least-squares polynomial coefficients. The coefficients are calculated using the least-squares criterion described by:

$$S = \sum_{i=1}^{N} \sigma_i^2 \tag{3.5}$$

where N is the number of calibration points used in the approximation and σ_i is the distance from each separate calibration point to the closest point on the calculated surface. The procedure will find the polynomial coefficients (a_0, a_1 and a_2) that minimize the sum of the square of the distances, σ_i. By entering the measured input coefficients

(b_α, b_β) into the calculated function f(b_α, b_β), interpolated values for α, β, θ, ϕ, A_t and A_s are obtained. The angle or pressure coefficient surfaces for the probe are assumed to be smooth locally and not exhibit any large gradients or discontinuities. The local least-squares method generates a surface that does not directly go through all the calibration data points, but is rather an average surface. A standard polynomial surface fit can exhibit large fluctuations because the surface is required to go through all the data points. The least-squares surface will moderate the effect of a badly selected or measured point and create the best overall surface fit.

The angles α, β and the pressure coefficients A_t, A_s are given directly by the least-squares interpolation. The total pressure and static pressure are calculated from the non-dimensional pressure coefficients A_t, A_s:

$$p_t = p_i - A_t \cdot q \tag{3.6a}$$

$$p_s = p_t - \frac{q}{A_s} \tag{3.6b}$$

For low speeds, i.e. for flows with Mach numbers below 0.2, We can than calculate the magnitude of the velocity in terms of the classical formula

$$U = \sqrt{\frac{2(p_t - p_s)}{\rho}} \tag{3.7}$$

For high subsonic speeds, one needs to measure the total temperature T_t. The velocity magnitude and the flow conditions are then calculated using adiabatic, perfect gas relationships for air. Mach number from total pressure and static pressure:

$$M = \sqrt{5 \cdot \left(\left(\frac{p_t}{p_s}\right)^{2/7} - 1\right)} \tag{3.8}$$

Temperature and velocity magnitude are calculated from:

$$T = \frac{T_t}{(1 + M^2/5)} \tag{3.9}$$

$$U = M \cdot \sqrt{\gamma \cdot R \cdot T} \tag{3.10}$$

The Cartesian velocity components are calculated from the following equations:

$$u = U \cdot cos\alpha \cdot cos\beta \tag{3.11a}$$

$$v = U \cdot sin\beta \tag{3.11b}$$

$$w = U \cdot sin\alpha \cdot cos\beta \tag{3.11c}$$

The viscosity is calculated from the Sutherland-law:

$$\mu = \mu_0 \cdot (\frac{T}{T_0})^{3}/_{2} \cdot (\frac{T_0+S}{T+S}) \tag{3.12}$$

Where S is the Sutherland constant. For air: S = 111 K, μ_0 = 1.1716E-5 m^2/s and T_0 = 273 K. Reynolds number per unit length:

$$\frac{Re}{1} = \frac{U \cdot \rho}{\mu} \tag{3.13}$$

3.4. Calibration in Supersonic Flow

When a Pitot tube is placed in a supersonic stream with Mach number M_1, a detached shock forms upstream of its tip. Let p_{o1} and p_{o2} be the total pressure in front and behind the shock wave respectively. The Pitot tube then records the quantity p_{o2}, and if p_{o1} is known, then the Mach number can be found by measuring the static pressure using the isentropic relationship

$$\frac{p_{o1}}{p} = (1 + \frac{\gamma-1}{2} M_1^2)^{\gamma}/_{(\gamma-1)} \tag{3.14}$$

which is valid for both subsonic and supersonic isentropic flow. The flow across the shock of course is not isentropic, but if a static pressure ring of a Pitot-static probe is far enough from the probe tip, then the local static pressure ahead of the shock is recovered. In the laboratory, p_{o1} is the reservoir pressure and can easily be measured, assuming the flow can reach the probe without passing through regions of non-isentropic motion, like boundary layers or shock waves. In the latter case, or in case the probe is inserted in a stream where the total pressure is not known, a more useful formula can be obtained by using the classical normal shock relationship to eliminate p_{o1} and arrive at the Rayleigh supersonic Pitot formula:

$$\frac{p}{p_{o2}} = \frac{(\frac{2\gamma}{\gamma+1}M_1^2 - \frac{\gamma-1}{\gamma+1})^{1/\gamma-1}}{(\frac{\gamma+1}{2}M_1^2)^{\gamma/\gamma-1}} \tag{3.15}$$

By measuring the probe tip pressure p_{o2} and the static ring pressure p , one can use this formula to calculate the stream Mach number. The problem is that this information is not enough to determine other flow quantities, like flow velocity. The dynamic pressure can be calculated.

$$q = \frac{1}{2}\rho V^2 = \frac{\gamma}{2}pM^2 \tag{3.16}$$

But the density is needed to determine the velocity.

The most effective method to return the velocity is to measure the local value of the total temperature, T_o , determine to local value of the speed of sound a_o

$$a_o^2 = \gamma R T_o \tag{3.17}$$

and then use the following relationship to calculate the local value of the velocity:

$$(\frac{V}{a_o})^2 = \frac{2}{(2/M^2)+(\gamma-1)} \tag{3.18}$$

Consider now a five-hole probe with pressures recorded along the center hole, 1 and the peripheral holes 2 through 5. For low incidences, pressure p_1 is essentially the total pressure behind the shock, denoted earlier by p_{o2} . Let the average of the peripheral port pressures be

$$p_a = \frac{1}{4}(p_2 + p_3 + p_4 + p_5) \tag{3.19}$$

Here p_a is the pseudo-static pressure. The quantities p_1 and p_a are related to the Mach number, but an analytical expression similar to Eq. (3.8) is very hard to obtain. In practice probes are calibrated to generate the dependence of the ratio p_a / p_1 to the Mach number. An example of such an experimentally-obtained relationship (Naughton et .al 1993) is presented in Fig. 13.

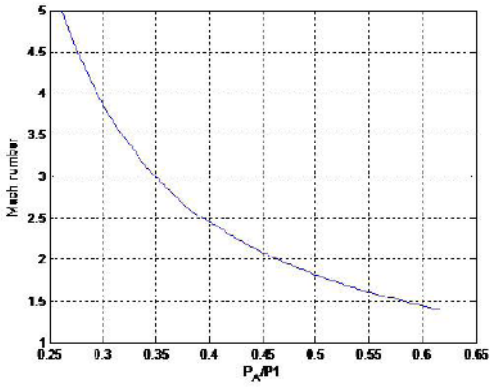

Figure 13. Dependence of p_a / p_1 to Mach number

Many authors (for example Naughton et .al 1993) demonstrated that for a wide range of supersonic Mach numbers the dependence of the pressure coefficients b_α and b_β (Eqs. 3.3 b and c) on pitch and yaw is very weak. But the quantity p_a / p_1 varies with the Mach number, pitch and yaw. This requires that for each Mach number correction factors be determined by the calibration process that are expressed as functions of pitch and yaw.

3.5. Calibration of High-Frequency-Response Probes

Recent advances in miniaturization of pressure transducers, including MEMS technology, have provided miniature, high bandwidth pressure transducers and transducer arrays well suited for fast-response, multi-hole probes. The miniature size of these arrays enables a design in which the transducers are embedded in, or close to the probe tip while maintaining a tip diameter of 1-2 mm. A number of researchers have designed fast-response, multi-hole probes to resolve unsteady flowfields (Senoo et al. 1973, Castorph and Raabe 1974, Kerrebrock et al. 1980, Matsunaga et al. 1980, Ng and Popernack 1988, Naughton et al. 1992, 1993, Roduner et al. 1998, 2000, Koppel et al. 2000, Kupferschmied et al. 2000). Kerrebrock et al. (1980) designed a probe with high frequency response (30 kHz), but with a large probe tip diameter (5 mm). Ng and Popernack (1988) developed a four-sensor probe with a diameter of 5.2 mm and a frequency response of 20 kHz. Matsunaga et al. (1980) developed a probe with small tip diameter (2 mm), but with a limited frequency response (500 Hz). Naughton et al. (1992, 1993) developed a 5-hole probe for supersonic flow measurements with a 1.1 mm probe tip, but frequency response limited to 50 Hz. In most of these efforts, the frequency response limitations were caused by the tubing leading from the probe tip to the pressure transducers mounted in the probe body.

Although the frequency response of such a probe is excellent, there are issues pertaining to fluid inertia-related unsteady aerodynamic effects that affect the pressures registered by the probe, and must therefore be taken into account in the calibration of the probe. The simplest framework to understand the origin of these fluid inertial effects is potential flow.

Consider a sphere in steady translation through an inviscid fluid at rest. The drag on this sphere is zero due to the equal and opposite pressure forces on the windward and the leeward sides of the sphere (d'Alembert's paradox). If the same sphere is in accelerated translation through the inviscid fluid, the pressure forces on the windward and leeward side no longer balance, and this results in net force acting in the direction opposite to the acceleration. A multi-hole probe in an unsteady flow field will also be subjected to these acceleration effects. This results in port pressures that are not only dependent on the dynamic pressure of the fluid and the tip geometry, but also on an additional term that is proportional to the flow acceleration (inertial or "added-mass" effects).

If one considers a sphere in accelerated translation through an infinite fluid at rest with a body-fixed reference frame, the instantaneous pressure on any point on the sphere surface is given by the unsteady Bernoulli equation (Karamcheti 1966):

$$P(\vec{r},t) = p_s - \rho\left[\frac{\partial \Phi}{\partial t} - \overrightarrow{U(t)} \cdot \nabla\Phi + \frac{1}{2}(\nabla\Phi)^2\right] \tag{3.20}$$

where p_s is the far-field static pressure. Equation 3.20 describes the pressure in terms of the position vector $\vec{r}$ and time, t. For a sphere, the flow field is axisymmetric and the position vector can be described in a spherical coordinate system in terms of r and θ. The perturbation potential, Φ, is a scalar the gradient of which yields the flow perturbation velocity. For a sphere, the perturbation potential is:

$$\Phi(\theta,t) = -\frac{1}{2}U(t)\frac{R^3}{r^2}cos\,(\theta) \tag{3.21}$$

where the radius of the sphere is given by R and U(t) is the time dependent velocity of the sphere. The pressure distribution on the sphere surface as a function of the sphere velocity and the angle θ is determined from Eq. 3.20 and Eq. 3.21:

$$C_p(\theta,U,t) \equiv \frac{p(\theta,U,t)-p_s}{\frac{1}{2}\rho U(t)^2} = \left(\frac{9}{4}cos^2(\theta) - \frac{5}{4}\right) + \frac{R}{U(t)^2}\frac{dU(t)}{dt}cos(\theta) \tag{3.22}$$

This pressure coefficient is based on instantaneous velocities that can be described is terms of a steady and an unsteady component:

$$C_p(\theta,U,t) \equiv C_{p_{STEADY}} + C_{p_{UNSTEADY}} \tag{3.23}$$

where:

$$C_{p_{STEADY}} = (\frac{9}{4}cos^2(\theta) - \frac{5}{4}), \qquad C_{p_{UNSTEADY}} = \frac{R}{U(t)^2}\frac{dU(t)}{dt}cos(\theta) = K(t)cos\,(\theta) \tag{3.24}$$

This is the pressure distribution on the surface of the sphere, moving at velocity U(t), in a fluid at rest. The same pressure distribution would also be seen if the sphere is stationary and the flowfield is moving with velocity -U(t). For steady flows, the inertial/unsteady term described by Eq. 3.24 vanishes and the pressure distribution on the sphere surface is given by just the steady component. However, for accelerated flows, the inertial term will be non-zero, and in the case of a multi-hole probe, corrections must be made to accurately resolve the flow properties from the measured port pressures. On the windward side of a sphere the viscous effects are small and the pressure distribution is similar to the inviscid prediction.

In the previous analysis, the stagnation point was known and fixed, therefore only one variable, the angle θ, was enough to describe the pressure anywhere on the sphere surface. Now, however, as the flow angle with respect to the probe axis changes, the stagnation point changes location as well. Thus, in order to describe the relative position of the stagnation point with respect to a pressure port, two variables, the pitch and yaw angles, α, β, are necessary. Also note that the pitch and yaw angles, α, β, are global with respect to the probe axis and not local, with respect to the individual ports:

$$C_p(\alpha,\beta,U,t)_i \equiv \frac{p_i(\alpha,\beta,U,t)-p_s}{\frac{1}{2}\rho U(t)^2} = C_{p_{STEADY\,i}} + C_{p_{UNSTEADY\,i}} \tag{3.25}$$

where i indicates the i[th] port of the multi-hole probe (for example, for a 5-hole probe, i takes values from 1 to 5) . For general, non-periodic flows, the instantaneous non-dimensional acceleration, K, is defined as:

$$K(t) = \frac{R}{U(t)^2}\frac{dU(t)}{dt} \tag{3.26}$$

With this, and in order to express Cp as a function of K(t), we rewrite Eq. 3.25 as follows

$$C_p\big(\alpha,\beta,K(t)\big) = C_{p_S}(\alpha,\beta) + K(t)C_{p_U}(\alpha,\beta) \tag{3.27a}$$

where :

$$C_{p_{STEADY}} = C_{p_S}, \qquad C_{p_{UNSTEADY}} = K(t)C_{p_U} \tag{3.27b}$$

and for the sphere:

$$C_{p_S} = \left(\frac{9}{4}cos^2(\theta) - \frac{5}{4}\right), \qquad C_{p_U} = cos\,(\theta) \tag{3.27c}$$

Note that the angle θ here is a function of α and β. For an actual probe, these coefficients are determined by combining experimental approaches with the theory described above. The non-dimensional acceleration, K, describes the magnitude of the unsteady or inertial effects on the probe. From the equations it can be seen that the

error made by ignoring the inertial term, is linearly proportional to K, or equivalently, linearly proportional to the probe size and the acceleration, and inversely proportional to the square of the velocity. To demonstrate the point, consider a probe with a tip diameter of 2 mm placed in an oscillating air stream at zero incidence. The flow velocity is taken to be sinusoidal with a frequency of 2 kHz, a mean of 20 m/s and 10% amplitude. The value of the non-dimensional acceleration coefficient is identical to the error in magnitude if the inertial effects are ignored. For our example, the calculated maximum K-value is 0.063, meaning that for the 2 mm probe in the described flowfield, a maximum measurement error in the predicted dynamic pressure of 6.3% is expected if the inertial effects are not accounted for. If the frequency is increased to 20 kHz the maximum error in the predicted dynamic pressure will increase to 63%.

In terms of the flow angles, for measurements in steady flows, steady probe calibration is first performed to determine the relationship between the port pressures and the flow incidence angle. The port pressures are used to form two non-dimensional pressure coefficients, b_α and b_β (see Eqs. 3.3 b and c) that describe this relationship. It was demonstrated experimentally (Johansen 2001) that these coefficients have very little dependence on the inertial effects for angles between –40 and 40 degrees, even for large values of K. This further enables the use of the steady calibration polynomial surface fits to be used in the prediction of the flow angles of an unknown, unsteady flow field. For higher angles, the unsteady effects should be taken into account.

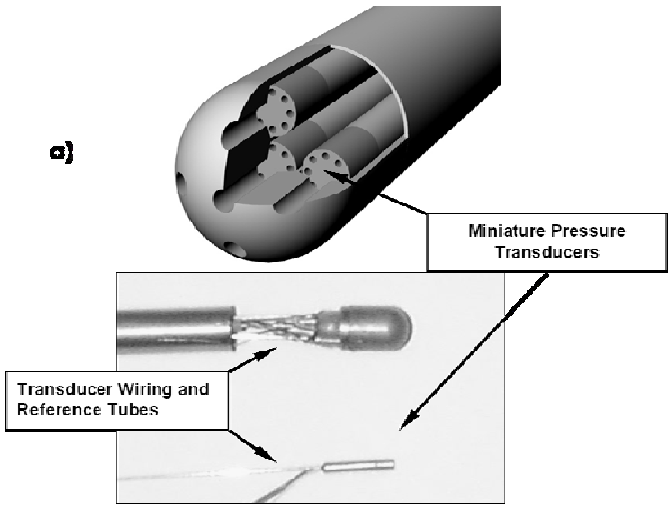

Figure 14. A 6.35 mm, 5-hole,fast-response probe. The probe has five Kulite XCS-062 transducers

However, correct measurement of the velocity magnitude requires exact quantification of the inertial effects. The velocity magnitude for a conventional (steady) multi-hole probe is generally calculated from the total and static pressures. These pressures are determined, via the probe's steady calibration, from the measured port pressures. For probe use in an unsteady flow field, the introduced procedure for determining the instantaneous velocity magnitude is described below. Here, and without loss of generality, the static pressure is assumed to be known, but not necessarily constant.

During data reduction, time series of the port pressures, $p_i(t)$, are recorded and the pitch and yaw angles are found for each time instant (from the previous section on flow angle determination). Based on these predicted angles, the steady and unsteady pressure coefficients are found from their respective polynomial expressions. The velocity is then found by solving Eq. 3a, which is a non-linear, first-order, ordinary differential equation. Such equations can easily be solved for a time series of data using a numerical method, such as the Runge-Kutta method.

The velocity magnitude correction algorithm was applied to a 0.25" O.D. embedded-sensor probe shown in Fig. 14, tested in a specially designed facility which can generate oscillatory velocity profiles with frequencies up to around 1kHz. Figure15 shows the exact velocity, measured by a hot wire as well as the uncorrected and corrected velocity profiles derived from the embedded sensor probe.

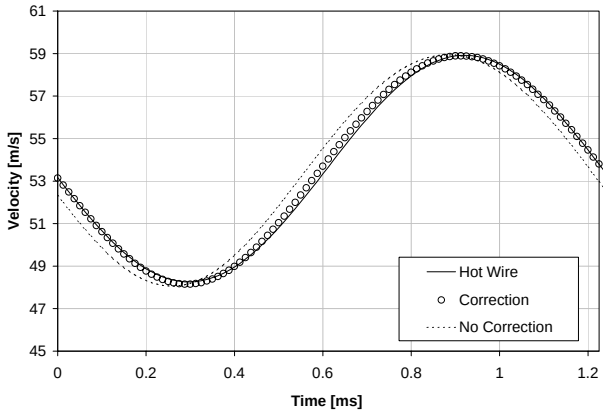

Figure 15. Ensemble averaged velocity from hot-wire, numerical correction routine, and center port pressure without inertial effect correction.

3.6. Error Analysis

Experimental error is defined as the difference between the measured value of a physical quantity and its true value. It is often necessary to estimate the error to be able to determine the confidence that the measured or predicted result is within a specified range of the true value. The expected errors from a measurement or prediction will be referred to as the uncertainty and can be estimated in several ways.

In estimating the uncertainty of measuring with multi-hole probes, the user will have to direct attention first to the problem of bias or systematic error, which is error that is roughly constant throughout the sampling of the data. Such errors can be due to errors in the reading of the reference manometer, hysteresis and temperature drift of pressure sensors and probe positioning and measurement. Bias errors are ignored in this analysis because the experimenter should identify them and they can be accounted for. Errors due to non-linearity and the averaged sequential recording of pressures are summed up in an uncertainty in the pressure reading. Here we will discuss errors due to the data reduction techniques and the interpolation routines.

When a physical quantity, R is estimated in terms of measured parameters, x_i, errors in the measurement of the quantities x_i propagate. It was demonstrated that the method of constant odds provides good accuracy in the estimate the uncertainty δR:

$$\delta R = [(\frac{\partial R}{\partial X_1}\delta X_1)^2 + (\frac{\partial R}{\partial X_2}\delta X_2)^2 + \cdots + (\frac{\partial R}{\partial X_n}\delta X_n)^2]^{1/2} \quad (3.28)$$

This method requires that each of the x_i's are independent variables and that they have a Gaussian error distribution.

In the present case the physical quantitiesα, β, θ, ϕ, A_t, A_s depend on the coefficients b_α, b_β, b_θ, b_ϕ, A_t and A_s. These coefficients are differentiated with respect to all the independents variables here the pressure measurements, $x_i = p_i$. Johansen et al.(2001) estimate the errors induced from using a linear least-squares interpolation technique. The surface fitting procedure in many conventional data reduction algorithms is found to be one of the greatest sources of error. A global surface fitting procedure will complicate the structure of the surface because the probe tip surface on a small probe usually contains irregularities that will be reflected in the measured pressures and non-dimensional coefficients. Even smaller sector sized surfaces have these problems when trying to fit an interpolation surface to all calibration points in that sector. A local least-squares approach can be more accurate, because the surface is only covering a small segment of the probe and uses few data points. A linear local least-squares surface can create a very good approximation to the actual data assumed that there is dense grid of calibration data.

A procedure to validate the accuracy of the LLS routine was performed using a known model surface. For each of the separate sectors on a 7-hole probe a surface was created using all the calibration data points belonging to that sector. A second order polynomial surface was created using surface fitting software. The resultant error (R^2) of approximating a second order surface over all the calibration data points in each sector was reasonably good. The second order surface will now be regarded as a model surface because it contains similar characteristics as would an actual calibration surface. Because the polynomial expression is known for the surface, a grid of angle coefficients is created with corresponding exact values for the angles. The new grid is created to have similar density and distribution of data points as the actual surface. For the created range of test points the exact values for the pressure coefficients and the angles are known through the four model surface polynomials. The new test file is reduced using a modified version of the LLS algorithm that only reads the test data coefficients and finds the closest (by Euclidean distance) 6 coefficients in the calibration file and interpolates the value for the test data angle. The error is calculated as the difference of the LLS calculated angle and the exact angle calculated by the polynomial expression for the model surface. The data reduction also selects which calibration points to use in the data reduction such that this method can also serve as a measure for the quality of the data point search routine.

As described the surface fit is most probably not a smooth 2nd order polynomial surface over an entire sector and the surface might exhibit larger curvature locally. Several “worst case” examples were analyzed by fitting a higher curvature surface through fewer data points. However, the results from this analysis found that the contributing errors due to the local least-squares surface fit are negligible. Discrepancies between the fitted surface and the model surface were on the order of 10^{-5} degrees for angle calculations and 10^{-3} percent for velocity calculations.

4. PROBE INTERFERENCE

Any probe inserted in the flow will interfere with the flow, and the readings of any probe will be influenced by the presence of bodies that are inserted in the flow. In most cases, such interference is negligible, but on occasion it may be considerable. In general, when the probe is placed in high receptivity areas, its effect on the flow may be from non-negligible to dramatic.

High receptivity regions of a flow are regions where bifurcations can easily occur through the introduction of a relatively small disturbance. In other words, these are areas where a small energy/disturbance input causes dramatic changes to the flow behavior. For example, the introduction of a small disturbance near the separation point has the potential of swinging the flow from fully separated to fully attach and vice versa. Placement of the probe in such regions is likely to affect the flow behavior.

The size of the probe and the hardware holding it in place is also an important factor. By adequately miniaturizing the probe and the associated probe holder/positioning hardware, it is possible to avoid such occurrences.

Probe Upstream of Body

If the probe is placed with its tip upstream of the body, there will be no interference on the readings of the probe. Within its own accuracy, the probe will read the flow features at the point it is placed, which are influenced by the body. The probe itself may introduce very small disturbances to the flow over the body. These will depend on the configuration under consideration. But if a probe is inserted close to the stagnation streamline (Fig. 16 position A), it is possible that disturbances may be introduced in the boundary layer, and induce transition to turbulence.

Probe Away from the Body

A probe placed in tandem with the body but five probe diameters away from its surface (Fig. 16 position D) will not introduce any interference, nor will its readings be affected by the body. But if a probe is placed within the boundary layer (Fig. 16 positions B and C), it may trip the boundary layer, induce transition to turbulence, and affect significantly the location of separation.

Probe in the Wake

A probe placed in the free-shear layer may trip it to turbulence and influence the rate at which this layer rolls to form large vortical structures. But in most practical cases for Reynolds numbers larger than one hundred thousands, shear layers are always turbulent. A probe placed in the wake (Fig. 16 position E) will have no effect on the flow. But it will not be able to provide good measurements, since the flow in this region may be reversed.

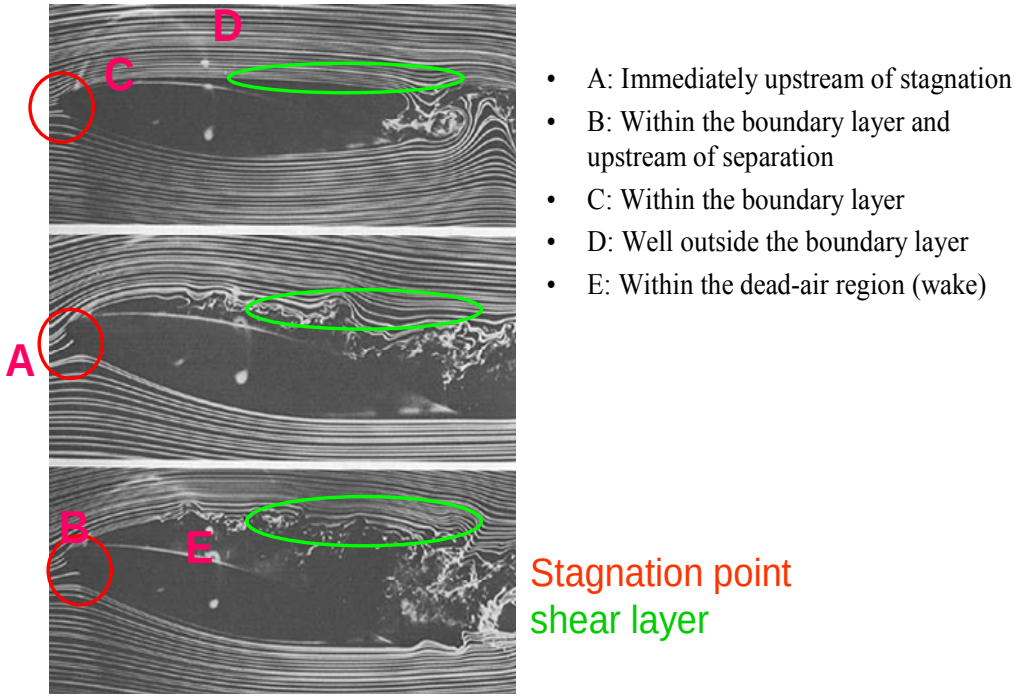

Figure 16. Regions of possible interference of probes with the flow

Probe in Three-Dimensional Flows.

The above statements are valid for flow over three-dimensional bodies. A special 3-D case is axial vortices, like wing-tip, or delta-wing vortices. Such swirling vortices may contain large axial and circumferential velocity components. A probe inserted close to the core of an axial vortex with its axis in line with the vortex axis may induce vortex breakdown, and alter drastically the flow. Another problem arises if the probe is inserted in an axial vortex with its axis in the circumferential direction. In that case, strong gradients of the circumferential velocity component give rise to radial pressure gradients, which are interpreted by the calibration software as large radial velocity components. These are often called phantom,

5. MHP USE AND APPLICATIONS

5.1. Laboratory Use

In the first few decades of laboratory work in aerodynamics, the Pitot-static probe was the only tool available to measure flow velocity. Five-hole probes followed soon. Then, more sophisticated methods like hot-wire

anemometry, laser-Doppler velocimetry and more recently particle-image velocimeter provided more options to the researchers. But with the development of miniature pressure transducers, powerful computers and sophisticated software led to the re-emergence of multi-hole probes. Today MHP compete with all other tools of flow measurement, and their ease of use and low price make them attractive to researchers and practicing engineers.

MHPs are used extensively in wind tunnels where they are first employed to calibrate the tunnels by recording the uniformity of the flow in the test section. Such probes can then be employed to map out the velocity field around aerodynamic models. They are often used to generate data along a grid in the wake of an aircraft model, which can then be used to estimate drag and lift, as well as the strength of the wing-tip vortices. But the same probes are often used to document the flow field around the model. MHPs are also used to explore the flow field around automobile models.

MHPs are also employed in turbomachinery applications. They can generate the flow properties downstream of the fan of a gas-turbine engine, between compressor stages, and even in the exhaust region. Here is where special MHPs like fast-response probes that capture many points within the period between two blade passages or high-temperature probes become very useful.

5.2. Field Measurements

Multi-hole probes are often employed for field measurements. They are often used by many different industries in monitoring smoke stack flows. They find applications in wind engineering, monitoring wind speed and direction. But the most important practical application is their use in detecting the pitch and you of aircraft. The MHP used in this application is called the “air-data probe. The tip of such a probe is essentially a conventional five-hole probe tip. But about ten diameters from the tip, air-data probes are usually equipped with a static ring, which consists of six to eight pressure ports that record the local static pressure by pneumatically averaging their readings.

6. REFERENCE

Allen, R., Traub, L., Johansen, E. S., Rediniotis, O. K. and Tsao, T., 2000, “A MEMS-Based 5-Sensor Probe,” AIAA-2000-0252, 38th Aerospace Sciences Meeting and Exhibit, Reno, NV, January 10-13.

Alexander A. Ned, Anthony D. Kurtz, Glenn Beheim, FawziaMasheeb, SorinStefanescu, “Improved SiC Leadless Pressure Sensors For High Temperature, Low and High Pressure Applications”, Twenty-First Transducer Workshop Lexington, Maryland, June 22-23, 2004

Bryer, D. W., and Pankhurst, R. C., “Pressure-Probe Methods for Determining Wind Speed and Flow Direction,” HMSO, (NPL), 1971.

Castorph, D., and Raabe, J., 1974, “Measurement of Unsteady Pressure Unsteady Relative velocity Field of a Kaplan Runner by Means of an Electronic Multi-miniature Probe as a Basic Contribution to Research on Unsteady Runner Load,” Proceedings of the 7th IAHR Symposium, Vienna.

Everett, K. N., Gerner, A. A. and Durston, D. A., 1983, “Seven-Hole Cone Probes for High Angle Flow Measurements: Theory and Calibration,” AIAA Journal, Vol. 21, No. 7, pp. 992-998.

Gossweiler, C.R. 1993, Sonden and Messsysteme fur Schnelle Aerodynamische Stroemungsmessungs mit Piezoresistiven Druckgebern, Dissertation, ETH, Zuerich, No 10253.

Heneka A., 1983, Development and Application of a Wedge Probefor Unsteady 3-D Flow Measurements. PhD thesis, University of Stuttgart.

Johansen, E. S., Rediniotis, O.K. and Jones, G.S., 2001, "The Compressible Calibration of Miniature Multi-Hole Probes" J. Fluids Eng. Vol. 123, pp. 128-137.

Johansen, E. S., 2001, "Development of a Fast-Response Multi-Hole Probe for Unsteady and Turbulent Flowfields," Ph.D. Dissertation, Aerospace Engineering Department, Texas A&M University, College Station, Texas.

Karamcheti, K., 1966, "Principles of Ideal-Fluid Aerodynamics," John Wiley & Sons Inc., New York.

Kerrebrock, J.L., Thompkins, W. T. and Epstein, A. H., 1980, "A Miniature High Frequency Sphere Probe," Proceedings of ASME Symposium on Measurement Methods in Rotating Components of Turbomachinery, pp. 91-98.

Koppel, P., Roduner, C., Kupferschmied, P. and Gyarmathy, G., 2000, "On The Development and Application of the Fast-Response Aerodynamic Probe System in Turbomachines – Part 3: Comparison of Averaging Methods Applied to Centrifugal Compressor Measurements," Journal of Turbomachinery, Vol. 122, pp. 527-536.

Kupferschmied, P., Koppel, P., Roduner, C. and Gyarmathy, G., 2000, "On The Development and Application of the Fast-Response Aerodynamic Probe System in Turbomachines – Part 1: The Measurement System," Journal of Turbomachinery, Vol. 122, pp. 505-516.

Kupferschmied, P., Koppel, P., Gizzi, W., Roduner, C. and Gyarmathy, G., 2000, "Time-Resolved Flow Measurements with Fast-Response Aerodynamic Probes in Turbomachines," J. Meas. Sci. Technol., Vol. 11, pp. 1036-1054.

Matsunaga, S., Ishibashi, H., and Nishi, M., 1980, "Measurement of Instantaneous Pressure and Velocity in Nonsteady Three-Dimensional Water Flow by Means of a Combined Five-Hole Probe," Transaction of the ASME Journal of Fluid Engineering, Vol. 102, pp. 196-202.

Naughton, J.W., Cattafesta III, L.N., and Settles, G.S., 1992, "A Miniature, Fast-Response 5-Hole Probe for Supersonic Flowfield Measurements," AIAA-92-0266, 30th Aerospace Sciences Meeting and Exhibit, Reno, NV, January 6-9.

Naughton, J.W., Cattafesta III, L.N., and Settles, G.S., 1993, "Miniature Fast Response Five-Hole Conical Probe for Supersonic Flowfield Measurements," AIAA Journal, Vol. 31, No. 3, pp. 453-458.

Ng, W.F. and Popernack, Jr., T.G., 1988, "Combination Probe for Hi-Frequency Unsteady Aerodynamic Measurements," IEEE Transactions on Aerospace and Electronic Systems, Vol. 24, No. 1, pp. 76-84.

Paniagua, G. and Denos, R., 2000, "Numerical Compensation in the Time Domain of Pressure Sensors," VKIRP 2000-59, Proceedings of the 15th Symposium on Measuring Techniques for Transonic and Supersonic Flow in Cascades and Turbomachines, Florence, Italy.

Rediniotis, O. K., Hoang, N. T., and Telionis, D. P., "The Seven-Hole Probe: Its Calibration and Use," Forum on Instructional Fluid Dynamics Experiments, Vol. 152, June 1993, pp. 21-26.

Rediniotis, O. K. and Pathak, M. M., 1999, "Simple Technique for Frequency-Response Enhancement of Miniature Pressure Probes," AIAA Journal, **37**, pp. 897-899.

Rediniotis, O. K., Johansen, E. S., Tsao, T., Seifert, A. and Pack, L. G., 1999, "MEMS-Based Probes for Velocity and Pressure Measurements in Unsteady and Turbulent Flowfields," AIAA-99-0521, 37th Aerospace Sciences Meeting and Exhibit, Reno, NV, January 11-14.

Roduner, C., Koppel, P., Kupferschmied, P. and Gyarmathy, G, 1998, “Comparison of Measurement Data at the Impeller Exit of a Centrifugal Compressor Measured with both Pneumatic and Fast-Response Probes,” ASME-98-GT-241, IGTI, Stockholm, Sweeden.

Roduner, C., Kupferschmied, P., Koppel, P. and Gyarmathy, G., 2000, “On The Development and Application of the Fast-Response Aerodynamic Probe System in Turbomachines – Part 2: Flow, Surge, and Stall in a Centrifugal Compressor,” Journal of Turbomachinery, Vol. 122, pp. 517-526.

Senoo, Y., Kita, Y. and Ookuma, K., 1973, “Measurement of Two-Dimensional Periodic Flow With a Cobra Probe,” Transactions of the ASME Journal of Fluid Engineering, pp. 295-300.

Sieverding, CH, Arts, T, Denos, R. and Broukaert, J.-F., 2000, “Measurement Techniques for Unsteady Flows in Turbomachines”, Experiments in Fluids, vol 28, pp. 285-321.

Zilliac, G. G., “Calibration of Seven-Hole Probes For Use in Fluid Flows With Large Angularity,” NASA TM 102200, December 1989.

7. RESPONSIBILITY NOTICE

The authors are the only responsible for the printed material included in this paper.